1 Nonlinear Compton data with green linear polarized laser and 46.6 GeV electron beam

Nonlinear Compton data were taken In August 1996 with green linear polarized laser incident on 46.6 GeV SLC electron beam.

Beam pipe on top of ECAL and vacuum chamber in front of ECAL were modified before the run in order to reduce backgrounds in ECAL. These modifications were modeled with GEANT v3.21 Monte Carlo and the following changes recommended by such optimization were made:

- Increase the vertical size of the beam pipe on top of ECAL from 4.5" to 8.0" in order to contain not only the original 46.6 GeV electron beam but also N=1 spectrum of scattered electrons. Electrons from interaction of 46.6 GeV electron beam with green laser involving only one laser photon (N=1 electrons) have much higher rate than electrons from N=3/N=4 spectrum at laser intensities $\eta = 0.2 - 0.3$ explored by this measurement. Crossing the beam pipe at small angles N=1 electrons produce significant background to N=3/N=4 measurements. This effect was observed in previous runs with IR laser when it significantly complicated measurements. After the increase of the diameter of the beam pipe from 4.5" to 8.0" part of the N=2 electron spectrum was also contained within the vacuum pipe making it impossible to do measurements in N=2 spectrum.

- Thickness of the beam pipe on top of ECAL was made as thin as possible. Beam pipe has the thickness 1/16" along the line where N=2 electrons cross the beam pipe.

- Thickness of the vacuum chamber in front of ECAL was reduced to 1/8".

- The vacuum flanges behind ECAL were moved as far from ECAL as possible. The flanges are part of the vacuum transition region necessary to separate electron and γ beams into separate lines after electron beam is bent by the permanent magnets. They contain significant amount of materials (Fe) and albedo from N=1 electrons hitting these flanges (backsplash) creates backgrounds in ECAL. This effect was also observed in previous runs with IR laser. Because flanges were moved farther from ECAL the albedo flux was reduced. In order to reduce it even more Pb absorbers (Pb-bricks) were placed between the vacuum flanges an ECAL below the path of N=1 electrons.

As a result of the above modifications backgrounds in ECAL were reduced by more than order of magnitude compared to the previous runs. Backgrounds represented only small fraction of the N=3,4 signal in ECAL and they were easily dealt with by reconstruction procedure described previously.

For the data analysis only those runs were used where ECAL was positioned at different vertical positions with 8mm steps - called ECAL scans. Because each ECAL scan has 10-12 steps these scans permit measurements of part of the spectrum reachable only by N=3,4 electrons within a single run. Position of the edges of the electron momentum spectrum reachable by N=1,2,3,4,5,6 electrons are defined by the following equation:

$$p_{e^-}^{(min)} = E_e \, \frac{1+\eta^2}{1+N\,x+\eta^2}$$

where parameter $x = 1.641$ for Green laser with $\omega = 2.35$ eV crossing 46.6 GeV electron beam at 17°. Position of the edges for $\eta = 0.14$ and $\eta = 0.30$ are calculated in Table 1.

Measurements by the top row of ECAL (row 1) for step $i+2$ overlapped with the second row (row 2) for step i. This allows a cross-check of the measurements and verification of the reconstruction procedure for different rows.

Each row of ECAL is a separate detector that samples part of the electron spectrum; the signal is maximum in the top-most row of ECAL and minimum in the lowest row. Because of the dynamic range of the calorimeter $\approx 10^3$ only four top rows measured significant signal; the typical ratio of the signals in rows 4 and 1 was 1:1000.

Reconstruction error was minimum for row 1. Signals in rows 2,3 and 4 have contribution from the leakage between rows and errors in signal reconstruction for these rows are significantly higher. In the final stage of the analysis only data from the row 1 of ECAL were analyzed and compared with simulations in the region of N=3,4 electrons because rows 2,3 and 4 repeated the same measurements with larger errors. Reconstruction of the low part of the spectrum for N=5,6 electrons that can be reached only by rows 3 and 4 was unreliable because of the low rate (less than 1 electron per electron-laser crossing) and comparably large backgrounds.

Laser energy was measured by the joule-meter in the laser diagnostic setup; laser focal area and pulse width measurements were unreliable. In order to reconstruct the laser intensity the nonlinear Compton rates from N=2 and N=3 electrons were measured by Cherenkov detectors installed in the path of scattered electrons. These detectors measure the total flux (not the energy flux) of electrons at momentum gaps that correspond to N=2 and N=3 nonlinear processes. N=2 and N=3 Cherenkov counters intercept the same electron spectrum

	$\eta = 0.14$	$\eta = 0.30$
N=1	17.86 GeV	18.60 GeV
N=2	11.05 GeV	11.62 GeV
N=3	8.00 GeV	8.45 GeV
N=4	6.27 GeV	6.64 GeV
N=5	5.15 GeV	5.46 GeV
N=6	4.37 GeV	4.64 GeV

Table 1: Position of the kinematic edges for N=1,2,3,4,5,6 electrons calculated for two field intensities $\eta = 0.14$ and $\eta = 0.30$. This edges were calculated for 46.6 GeV electron beam and green laser 2.35 eV crossing the electron beam at 17°; corresponding parameter $x = 1.641$.

that is incident to the ECAL but counters are located in more energetic part of the spectrum. However contrary to ECAL, N=2 and N=3 counters don't provide reliable measurements of the rate of electrons at fixed electron momenta. This is due to the uncertainty in the counter positions and their momentum calibration. Then their ratios were used to extract laser focus parameters (together with N=1 counter) as it will be explained in the section on positron analysis. As a result of the constraining procedure described in the positron section actual absolute signals in N=2,3 counters were different from one predicted by simulations by large factor - up to 10. Hence these counters can not be considered as independent measurement of the electron spectrum in N=2,3 region while ECAL does provide such measurements in N=3,4 region. Even if these counters measured the rate of electrons correctly they would represent measurements of the electron spectrum only at two additional points while ECAL measures the entire nonlinear Compton spectrum reachable by N=3,N=4 electrons.

1.1 Event selection

Events were selected according to the following criteria:

- Electron beam cut. Electron beam parameters were required to be within $\pm 3\sigma$ of their normal values for each run. Parameters include electron beam positions x and y, angles x' and y', beam current, beam energy, accelerator beam phase and the difference in accelerator current measured by two independent toroids. The last cut was necessary to check if the beam was partially lost or scattered in the FFTB between two measurements - important precondition to eliminate background from electrons of the beam scattered in the beam pipe ahead of the detectors.

- Laser cut. Laser diagnostics show a normal conditions with a measurement of the laser intensity available.

- Overlap cut (overlap between electron and laser beams due to timing). $\frac{N_\gamma^{(measured)}}{N_\gamma^{(simulated)}} > 0.7$: the ratio of the measured γ-flux to the simulated one without accounting for jitter was required to be more than 0.7. The distribution of the above ratio for one run is shown in Fig. 1. The ratio represents effective overlap between electron and laser beams. It should be 1 if $N_\gamma^{(simulated)}$ were calculated correctly and there was perfect overlap between electron and laser beam (peak densities of both beam occur at the same time at the same point). The fact that peak value (≈ 1.3 for the run presented in the example) is different form 1 is due to unknown error in electron beam parameters for each individual run. Only the average parameters of the electron beam were known and were used for calculation of $N_\gamma^{(simulated)}$. Overlap factor below 1 is due to the time jitter in electron-laser overlap that reduces the measured γ-flux $N_\gamma^{(measured)}$.

- DAQ cut. No unusually long trigger delay between two readouts was observed. This condition helps to avoid long pauses in DAQ readout due to the beam loss that sometime confused the DAQ system. In addition after the beam loss accelerator starts a new cycle with an unstable electron beam that can produce unusually large backgrounds. The above condition ensures that data were taken in a normal way as a continuous stream without interruptions.

- ECAL cut. Events were discarded if ECAL was saturated. Saturation in ECAL occurs if more than 10 TeV energy is deposited in one row due to dynamic range of the electronics. Individual channels of ECAL (each row is sum of 6 channels) saturate at $\approx$ 6 TeV . The signal is considered to be dangerously high if more than 2 channels measure energy deposition above 3 TeV - such events were discarded.

1.2 Correction for the leakage in ECAL

Correction for the leakages due to electromagnetic shower profile in ECAL was done according to procedure described in the preceding sections. Background subtraction was also done to take into account possible backgrounds from $N = 1$ electrons scattered in the same laser focus and rescattered into ECAL by different absorbers. We should note that due to improved beam pipe geometry backgrounds in ECAL were negligible in $N = 3, 4$ regions. Example of the signal in the outer pads of ECAL compared to one in central pads is shown in Fig. 2 for two different laser intensities.

There is a unique correspondence between momentum of an electron originated in the laser focus and vertical position of the ECAL row this electron is incident on. Electrons with higher momentum have higher vertical incident position, with lower momentum - lower

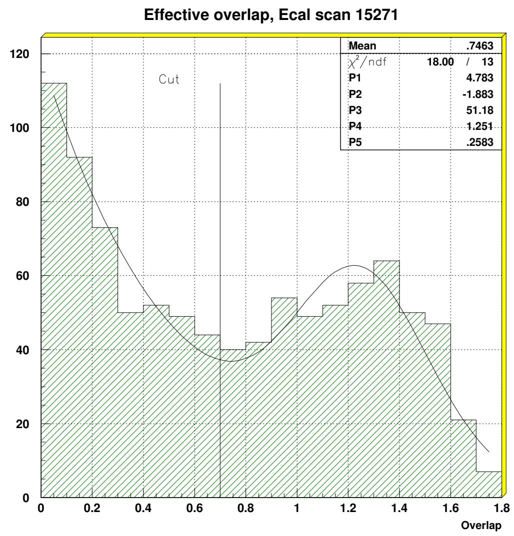

Figure 1: Ratio $\frac{N_\gamma^{(measured)}}{N_\gamma^{(simulated)}}$ for the ECAL scan 15271. Cut in overlap parameter 0.7 is also shown. Curve represents the fit of the data by exponent plus Gaussian distribution - two first parameters are for the exponent, the next three for the Gaussian fit.

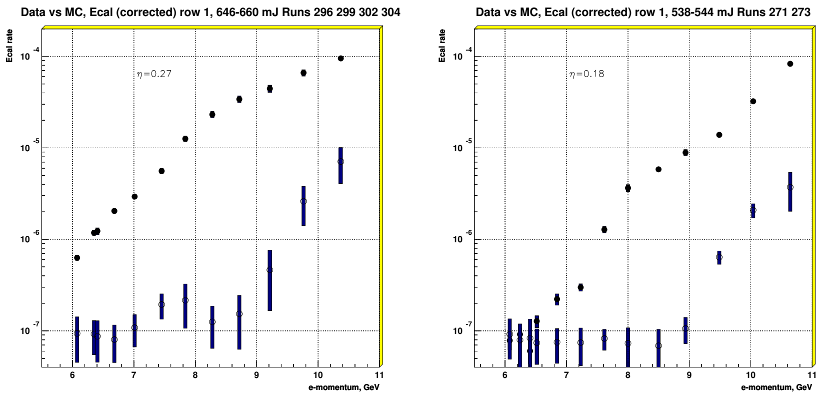

Figure 2: Reconstructed ECAL spectrum in central pads of ECAL (solid circles) and background in outer pads of ECAL (open circles with error bars) versus momentum of electrons originated in the laser focus and bended by the magnet. Plotted ECAL rate $\frac{1}{N_\gamma}\frac{dN_e}{dp}$ is the rate of electrons per unit momentum bin normalized by the measured γ flux N_γ. Two sets of runs with different laser intensities are shown: $\eta = 0.27$ (left plot) and $\eta = 0.18$ (right plot).

vertical incident position. The data (ECAL rate) are normalized to the measured γ-flux N_γ according to the formula:

$$\textbf{ECAL rate} = \frac{1}{N_\gamma}\frac{dN_e}{dp}$$

Two sets of runs with different laser intensities are shown in Fig. 2: $\eta = 0.27$ and $\eta = 0.18$. Because both signal and background are normalized to the γ-flux the normalized background is almost the same for two laser conditions (backgrounds are proportional to $N = 1$ electron rate) though the signal changes by order of magnitude.

These plots show that normalized background is decreases rapidly to the level of 10^{-7} electrons/1GeV/1γ at $p_{e^-} \approx 9$ GeV and then does not change. Because the nonlinear Compton signal is rapidly decreases with momentum to the same level 10^{-7} for $p_{e^-} < 6$ GeV it becomes smaller than background. Measurements in the region $N = 5, 6$ ($p_{e^-} < 6$ GeV) were not included in the analysis because of the comparably large background in this region and also because the electron rate drops below 1. For electron rates much smaller than 1 the average values of the energy deposition could not be calculated because due to the electronics noise and backgrounds the error is larger than the signal. Instead electron cluster reconstruction procedure must be employed if possible for $N = 5, 6$ region of ECAL. Unfortunately cluster reconstruction in this region gives unreliable results because of the much higher electron flux incident at ECAL only a few centimeters away.

1.3 Weighting of different events in data samples

Data were grouped according to the laser intensity η and momentum of the electrons incident at the center of the ECAL rows.

Data were grouped in 9 intervals for laser intensity η with $\Delta\eta$ in steps 0.02 from $\eta = 0.14$ to $\eta = 0.32$. These intervals allow η to vary ± 0.01 within each interval while the error in η reconstruction was $0.012 \leq \sigma_\eta \leq 0.025$ with most probable $\sigma_\eta = 0.018$. Error in η reconstruction is the estimated difference between actual η_{act} and $\eta_{reconst}$ from the measurements in $N = 2, 3$ monitors. Hence the uncertainty in η within each bin is dominated by the reconstruction error and not by the bin size. Reconstructed error σ_η versus η is plotted in Fig. 3.

Electron momentum bins were chosen in the range $p_{e^-} = 6 - 11$ GeV (N=4,3 range) with ± 0.2 GeV bin size around the central value. Data were taken at fixed ECAL positions that overlaps for different ECAL scans and most of the events within one bin have much smaller than ± 0.2 GeV variation around the central value of the bin momentum.

After selecting bins in η and electron momentum p_{e^-} events were plotted for each bin (η, p_{e^-}) (there were total ≈ 100 bins) and compared with simulated distributions. Signal distributions for $\eta = 0.19$ and different p_{e^-} bins are shown on Fig.4. Hatched histograms show measurements, not hatched - simulated events. Horizontal axis is the ECAL rate $\frac{1}{N_\gamma}\frac{dN_e}{dp}$. Measured and simulated events have similar distributions with essentially non-Gaussian shape. To compare measurements and simulated distributions average values and RMS of such distributions are calculated.

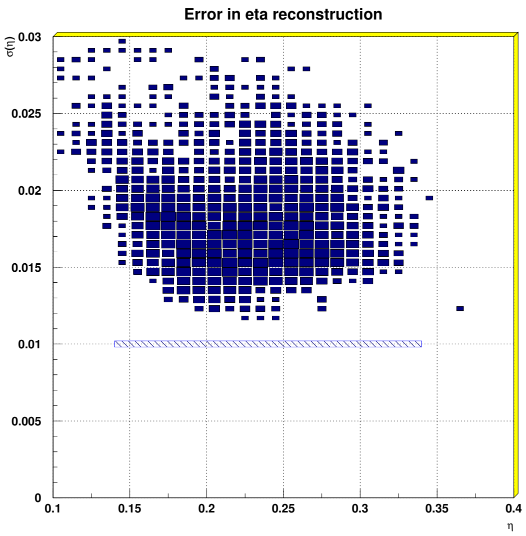

Figure 3: Error in η reconstruction for different η values is shown by boxes for different reconstructed events. Variation in η due to the final bin size 0.01 is smaller, it is shown for comparison as a line below the distribution.

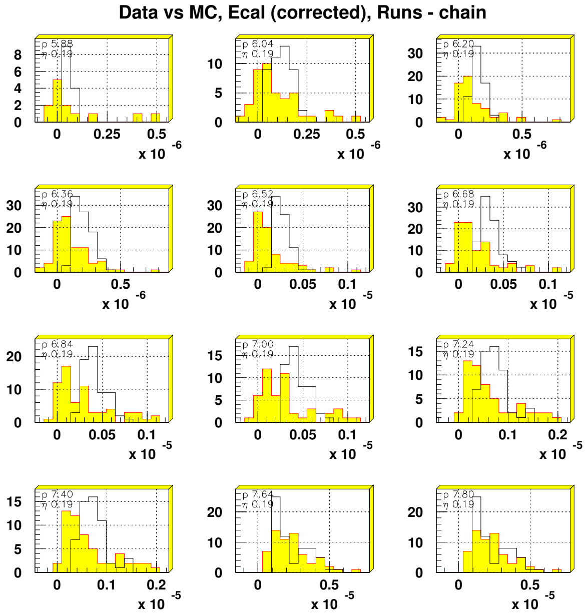

Figure 4: Measured (hatched histograms) and simulated (non-hatched histograms) distributions for $\eta = 0.19 \pm 0.01$ and p_{e^-}=5.88, 6.04, 6.20, 6.36, 6.52, 6.68, 6.84, 7.00, 7.24, 7.40, 7.64, 7.80 GeV. Horizontal axis is ECAL rate $\frac{1}{N_\gamma}\frac{dN_e}{dp}$. All ECAL scans data.

Average value is calculated according to:

$$< S >= \frac{\sum_i w_i \, s_i}{\sum_i w_i}$$

where w_i - weights attributed for each event, s_i - measured signals.

For simulated distributions there are no statistical errors for predicted ECAL rates if laser an electron beam parameters are known. Simulation results depend only on the laser and electron beam parameters. For finding the average and RMS all simulated events within each bin (η, p_{e^-}) were weighted with equal weights $w_i = 1$.

For measured distributions reconstruction procedure provides errors δs_i for the reconstructed signal in ECAL - those errors are dominated by the resolution of the calorimeter, leakages between rows and backgrounds. In average data have almost constant **relative** errors $(\dfrac{\delta s_i}{s_i} \approx Const)$ within a wide range of ECAL signals. But constant relative errors means that **absolute** errors are larger for larger ECAL signals. If measured distributions that have wide non-Gaussian shape were weighted with such errors $w_i = \dfrac{1}{\delta {s_i}^2}$ then the average will be much lower than one found for similar simulated spectrum.

We illustrate that with the following example. Suppose ECAL measures two events: 1000$\pm$100 GeV and 100$\pm$10 GeV. Then the weighted with errors average will be $< S >= 110$ GeV while uniformly weighted average will be $< S >= 550$ GeV.

To compare measured and simulated distributions they have to be weighted with the same weights. Below we provide arguments showing that for nonlinear Compton measurements events should be weighted with equal weights ($w_i = 1$) to find the better estimate of the central value for each distribution.

Equal weights should be used for the data sample selected after cuts; these cuts should also include cut on the error of the reconstructed signal to verify that the reconstruction procedure didn't fail.

If we assume that laser parameters such as η, focal area, focal width, laser energy fluctuate around some central values with Gaussian distributions then nonlinear Compton processes which have strongly nonlinear dependence on the above parameters (η^6, η^8 for $N = 3, 4$) will have non-Gaussian distributions with most probable values shifted to the lower values. Example of such distributions that corresponds to $\sigma_{\eta^2} = 22\%$ variation of η^2 around its central value $\eta^2 = 0.1$ are shown in Fig. 3. $\eta^2 = 0.1 \pm 0.022$ corresponds to $\eta = 0.32 \pm 0.011$ which is even lower than error $\delta\eta = 0.18$ shown in Fig. 5. N=1,2,3,4,5,6 signals that correspond to $\eta^2 = 0.1$ were assumed to be equal 1. The resulting distributions for N=3,4 signals in this example have distributions similar to the experimental data Fig. 4 with some events much higher than the central value 1.

As an example we weighted these distributions with equal weights $w_i = 1$ and with weights $w_i = \dfrac{1}{\delta s_i^2}$. The average values using two different weights are summarized in Table 2 (note that 1 corresponds to the $\eta^2 = 0.1$ in this example).

From this table one can see that average values for N=2,3,.. using equal weights are

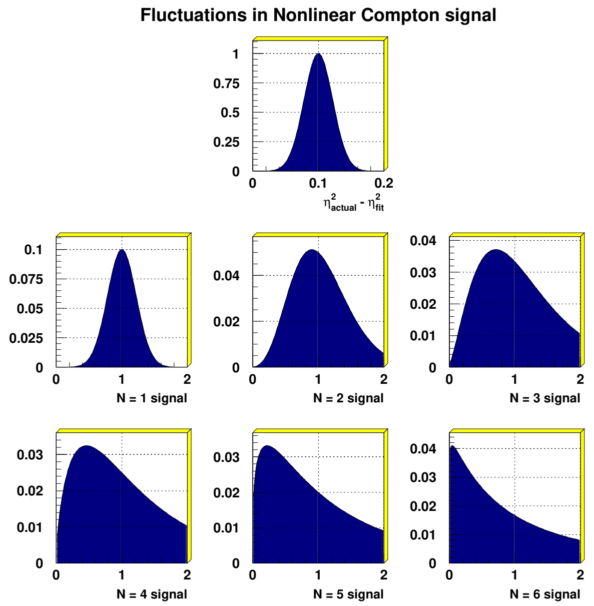

Figure 5: Plot on the top: assumed Gaussian fluctuation of the η^2_{actual} with $\sigma\eta^2_{actual} = 0.022$ around central value $\eta^2_{fit} = 0.1$. Six bottom plots: Simulated N=1,2,3,4,5,6 distributions that correspond to such fluctuations in η^2_{actual}. Signals are equal to 1 for $\eta^2_{actual} = 0.1$

slightly biased to the higher values. For arbitrary $\delta\eta^2$ the average value will be biased to:

$$\begin{aligned}
N &= 1 \qquad\qquad < S >= 1\,, \\
N &= 2 \qquad\qquad < S >= 1 + \left(\frac{\delta\eta^2}{\eta^2}\right)^2\,, \\
N &= 3 \qquad\qquad < S >= 1 + 3\left(\frac{\delta\eta^2}{\eta^2}\right)^2\,, \\
N &= 4 \qquad\qquad < S >= 1 + 6\left(\frac{\delta\eta^2}{\eta^2}\right)^2 ..
\end{aligned}$$

Average values found with error-weighting are scaled by much more significant factors ≤ 0.1 from the expected value 1 and these factors strongly depend on the $\delta\eta^2$ values. One can expect that the average value found with error-weighting will be much lower than the central value expected for some distribution and hence will give a very bad estimate. For equal-weighting the average value will be slightly higher than the central value by factor less than 2 and hence will give a good estimate of the central value (within this factor). In addition error-weighting average will have much larger fluctuations compared to the central value than equal weighting average due to unknown variation for the error $\delta\eta^2$ for each distribution.

	equal weights $w_i = 1$	weights with errors $w_i = \frac{1}{\delta^2_{s,i}}$
N=1	1.00	0.89
N=2	1.04	0.62
N=3	1.14	0.32
N=4	1.29	0.12
N=5	1.50	0.035
N=6	1.80	0.010

Table 2: Average values for N=1,2,3,4,5,6 distributions using equal weights (first column) and error-weighting (second column). Calculations are based on the assumption that $\eta^2)actual$ fluctuates around its central value $\eta^2_{reconstructed} = 0.1$ with $\delta\eta^2) = 0.022$. 1 corresponds to the central value $\eta^2 = 0.22$

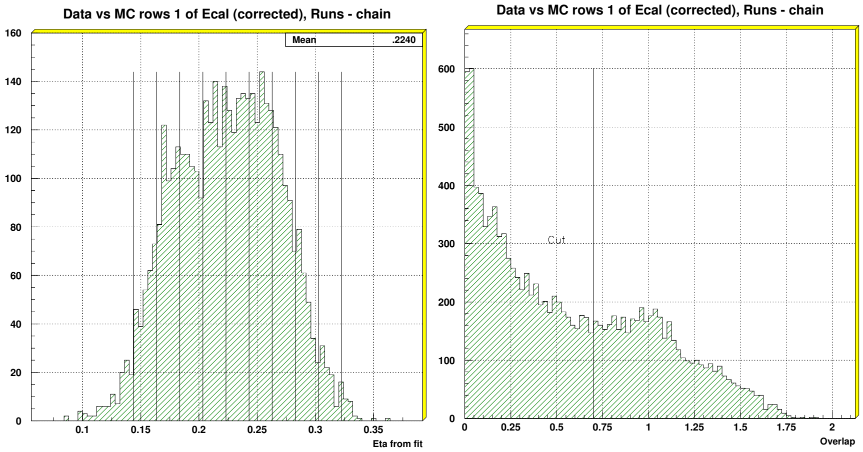

Figure 6: First plot: distribution of the laser intensity η with 9 bins selected. Second plot: distribution of the overlap parameter $\frac{N_\gamma^{(measured)}}{N_\gamma^{(simulated)}}$. Cut 0.7 is also shown as vertical line (only events above the cut were accepted for the analysis).

1.4 Nonlinear Compton rate versus electron momentum p_{e^-} and laser intensity η

More than 5000 events from 16 ECAL runs were analyzed. Laser intensity η distribution and distribution of the overlap parameter $\frac{N_\gamma^{(measured)}}{N_\gamma^{(simulated)}}$ for these runs are shown in Fig.6.

Data were selected using cuts as described earlier.

Data were combined in bins ($\eta \pm 0.01$, $p_{e^-} \pm 0.2$ GeV); only those bins that contain more that 5 events were analyzed and compared with simulations in order to avoid large error due to fluctuations in small data samples.

Equal weighting $w_i = 1$ was used for all events to find the average and RMS. Errors were calculated as $\frac{\text{RMS}}{\sqrt{N}}$, where N is the number of events. These errors underestimate the actual errors by a factor ≈ 2 because measured distributions were different from Gaussian. But due to the low statistics for some points and different spectra we do not speculate on the exact value of this factors and use the normal errors.

Data - number of electrons measured by the ECAL row - were normalized to the number of $N = 1$ photons and to the momentum acceptance of the row:

$$\textbf{ECAL rate} = \frac{1}{N_\gamma}\frac{dN_e}{dp}$$

Measurements were compared with simulations for different η values versus electron momentum p_{e^-}. Nine plots that shows this comparison are shown on Fig.8. All plots have the same vertical range 10^{-8} to 10^{-3} 1/GeV and the same horizontal range $p_{e^-} = 4 - 12$ GeV. Solid circles show measurements, open circles - simulation results. The same data in larger format are shown in Fig. 9 and Fig. 10.

Measurements were also compared with simulations for different momentum bins p_{e^-} versus laser field intensity η. Nine plots are shown on Fig.11. All plots have the same relative vertical range 200 (absolute ranges are different). Horizontal range $\eta = 0.14 - 0.40$. Solid circles show measurements, open circles - simulation results. The same data in larger format are shown on Fig.12, Fig.13 and Fig.14.

1.5 Discussion of results, comparison with simulation

Data presented above were compared with simulations for each bin η, p_{e^-}. Because within each bin laser parameters such as laser intensity η, laser area and laser pulse width were distributed differently simulations results don't correspond to a single continuous curve. No attempt has been made to scale laser parameter to the standard one in order to plot continuous distributions.

For the estimated error in the laser intensity $\frac{\delta\eta^2}{\eta^2} \approx 22\%$ expected uncertainty in the simulated $N = 3, 4$ rates is of the order of 2. Measurements agree with simulations within this error for all data points.

Electron spectra for small laser intensities $\eta = 0.15 - 0.20$ shown in Fig. 9 have a distinct plateau in the region $p_{e^-} = 8 - 10$ GeV that corresponds to the N=3 electron region. They show transition to the N=4 electron region below 8 GeV and N=4 region itself. Due to acceptance of the ECAL row $\Delta p_{e^-} = 0.5 - 1.4$ GeV measurements always represent smearing of the actual electron spectrum over the momentum acceptance of the row (Fig. 7). Due to the smearing N=4 plateau is not visible (compare Fig. 10) .

Dependence of the electron rates versus laser intensity η shows expected power laws. Note that η dependence in the Compton signal which normalized to the $N = 1$ rate manifest nonlinearity of the process.

In the $N = 4$ region (Fig. 12 $p_{e^-} = 6.0 - 6.7$ GeV) ECAL rate follows the power law $\eta^{4.8-5.0}$ in agreement with simulations. It is not exactly η^6 because acceptance of the ECAL row for N=4 electrons changes with η - ECAL measures different parts of N=4 spectrum for different η.

In the $N = 3$ region (Figs. 13 and 14 $p_{e^-} = 8.3 - 9.7$ GeV) ECAL rate follows the power law $\eta^{3.0-4.0}$ in agreement with simulations. It is again not exactly η^4 because acceptance of the ECAL row for N=3 electrons changes with η - ECAL measures different parts of N=3 spectrum for different η.

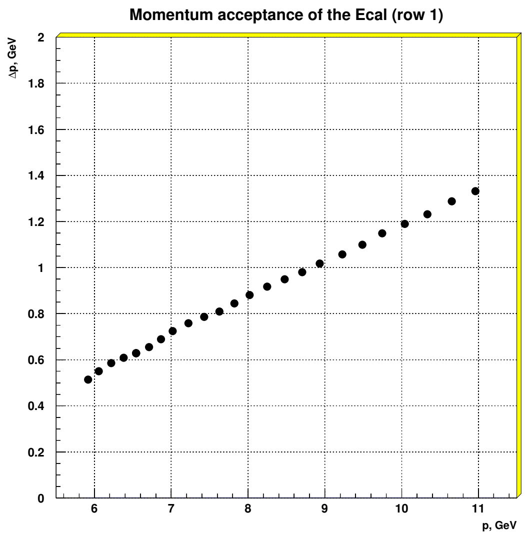

Figure 7: Momentum acceptance of the ECAL (GeV, row 1) versus the incident momentum (GeV). Smearing of the signal within each row acceptance is taking place - important effect in N=3,4 regions.

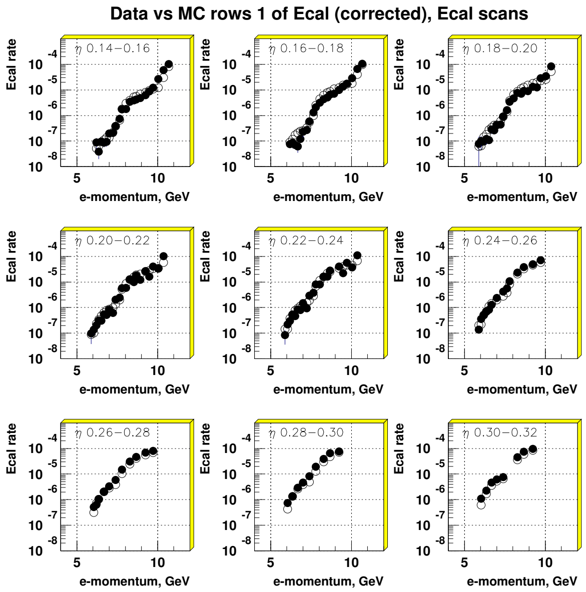

Figure 8: ECAL spectrums $\frac{1}{N_\gamma}\frac{dN_e}{dp}$ versus electron momentum p_{e^-} are plotted for 9 different η values in the range $\eta = 0.14 - 0.32$. Solid circles shows measurements, open circles - simulated results for the same laser parameters.

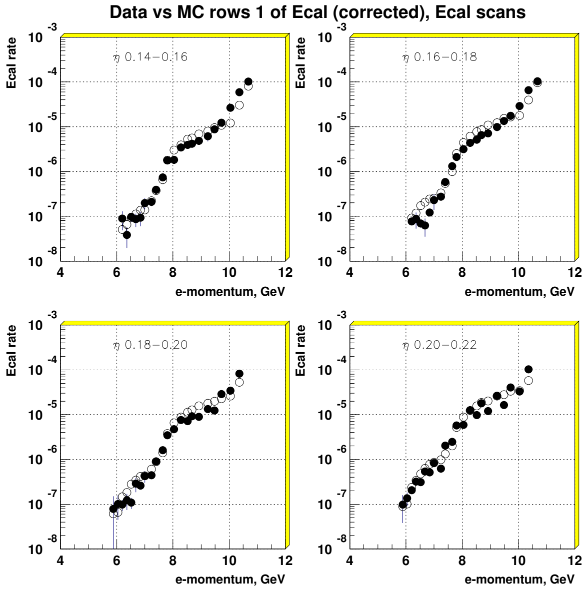

Figure 9: ECAL spectrums $\frac{1}{N_\gamma}\frac{dN_e}{dp}$ versus electron momentum p_{e^-} are plotted for 4 different η values in the range $\eta = 0.14 - 0.22$. Solid circles shows measurements, open circles - simulated results for the same laser parameters.

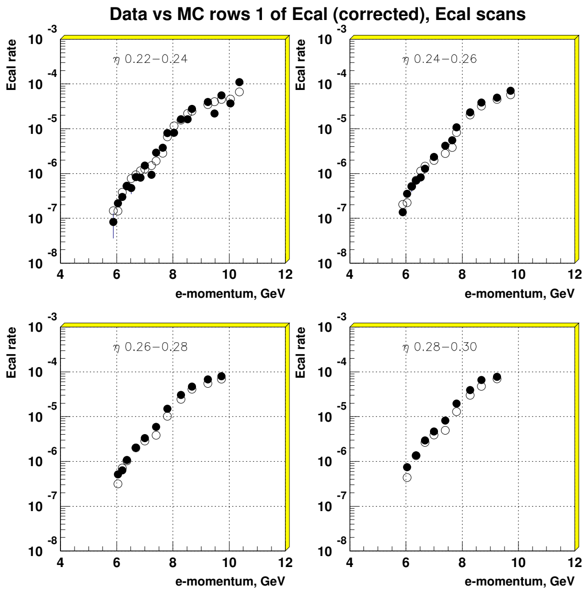

Figure 10: ECAL spectrums $\frac{1}{N_\gamma}\frac{dN_e}{dp}$ versus electron momentum p_{e^-} are plotted for 4 different η values in the range $\eta = 0.22 - 0.30$. Solid circles shows measurements, open circles - simulated results for the same laser parameters.

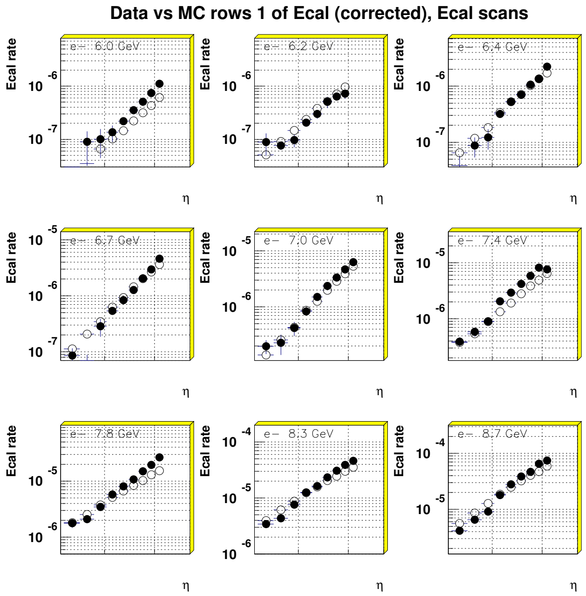

Figure 11: ECAL spectrums $\frac{1}{N_\gamma}\frac{dN_e}{dp}$ versus laser field intensity η are plotted for 9 different electron momentums p_{e^-} in the range $p_{e^-} = 6.0-8.7$ GeV. Solid circles shows measurements, open circles - simulated results for the same laser parameters.

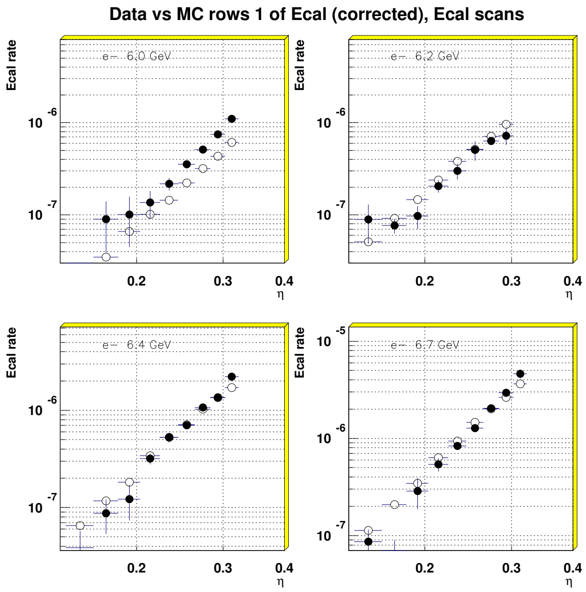

Figure 12: ECAL spectrums $\frac{1}{N_\gamma}\frac{dN_e}{dp}$ versus laser field intensity η are plotted for 4 different electron momentums p_{e^-} in the range $p_{e^-} = 6.0-6.7$ GeV. Solid circles shows measurements, open circles - simulated results for the same laser parameters.

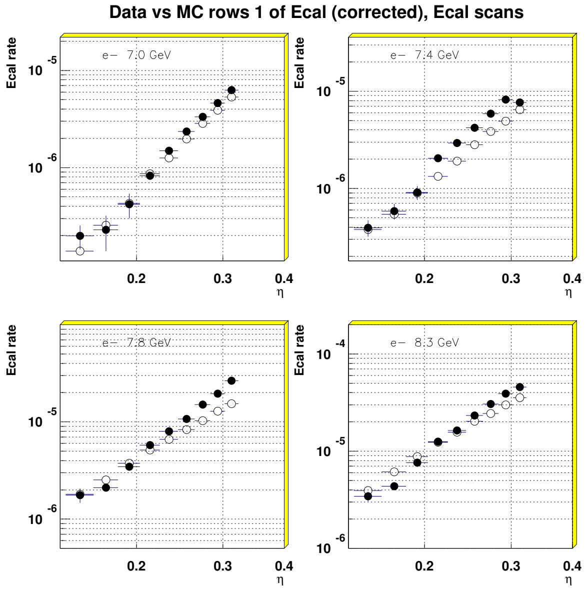

Figure 13: ECAL spectrums $\frac{1}{N_\gamma}\frac{dN_e}{dp}$ versus laser field intensity η are plotted for 4 different electron momentums p_{e^-} in the range $p_{e^-} = 7.0-8.3$ GeV. Solid circles shows measurements, open circles - simulated results for the same laser parameters.

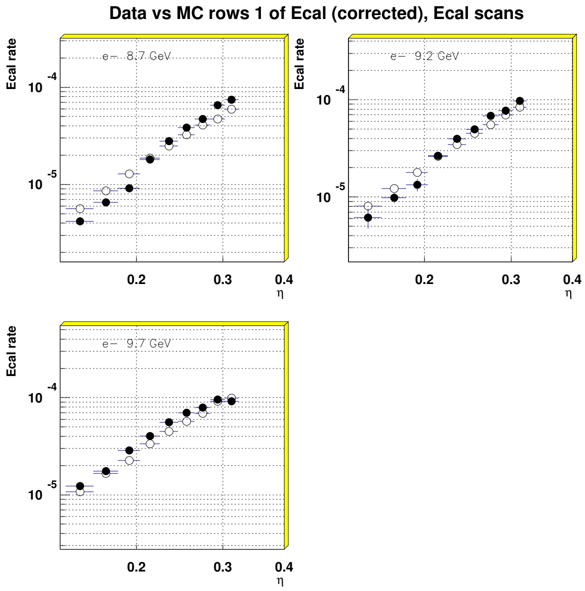

Figure 14: ECAL spectrums $\frac{1}{N_\gamma}\frac{dN_e}{dp}$ versus laser field intensity η are plotted for 3 different electron momentums p_{e^-} in the range $p_{e^-} = 8.7-9.7$ GeV. Solid circles shows measurements, open circles - simulated results for the same laser parameters.